Principle, Design, and Prototyping of Core Selective Switch Using Free-Space Optics for Spatial Channel Network

Masahiko Jinno, *Fellow, IEEE*, Takahiro Kodama, *Member, IEEE*, and Tsubasa Ishikawa

***Abstract*—We describe the principle, design, and prototyping of a free-space-optics-based core selective switch (CSS) for spatial channel (SCh) networks (SCNs) in the age of space division multiplexing (SDM). A CSS in an SCN corresponds to a conventional wavelength selective switch (WSS) in a current wavelength division multiplexing network. It incorporates functionalities for spatially demultiplexing SChs from an input SDM port and for switching and multiplexing any of them into any of output SDM ports. We discuss the design for free-space-optics-based CSSs that is applicable to CSSs supporting various numbers of cores per multicore fiber (MCF) and various numbers of MCF ports. We show an example of an implemented 5-core 1 × 6 CSS prototype that integrates an MCF collimator, spatial multiplexer/demultiplexer array, and liquid-crystal-on-silicon spatial light modulator. Although some output MCF ports exhibit relatively high insertion loss (IL), the CSS prototype shows that a CSS will potentially provide low net IL at the level of approximately 2 dB. To verify that there are no unknown deteriorating factors in the CSS prototype, we tested the prototype implemented in a hierarchical optical cross-connect configuration by measuring the pre-forward error correction bit error rate. Spatial bypassing and spectral grooming of a 900-Gb/s SCh employing a CSS-based spatial cross-connect and a conventional wavelength cross-connect are successfully demonstrated with no optical signal-to-noise ratio penalty.**

***Index Terms*—Core selective switch, Spatial channel, Spatial bypass, Spatial cross-connect, Spatial division multiplexing.**

I. Introduction

In order to support the ever-increasing demand for transmission capacity in optical networks while overcoming the fundamental capacity limits of conventional single-mode fibers (SMFs), research over the past 10 years has focused on exploring space as the only remaining physical dimension for signal multiplexing [1]. A near-term solution would be to use existing parallel SMFs. As middle or long-term solutions, a wide variety of fibers of new structures are being developed worldwide that support multiple guided spatial modes in a fiber. Now we are about to enter a new era of space division multiplexing (SDM). A multicore fiber (MCF) is one such SDM fiber in which multiple single-mode cores are placed within a single fiber cladding [2]. In general, MCFs are carefully designed to suppress the crosstalk between cores below the level allowed by the transmission system. They are advantageous due to their compatibility with the conventional SMF-based technology in terms of not requiring complicated multi-input multi-output digital signal processing for the spatial demultiplexing [3].

Although SDM fiber technology significantly scales in spatial mode counts per link and network capacity, it presents a challenge in that it necessitates the deployment of large reconfigurable optical add drop multiplexers (ROADMs) comprising a large number of high port count wavelength selective switches (WSSs). In order to address this problem, considerable research efforts have been dedicated to developing mixed-layer larger-scale wavelength division multiplexing (WDM)/SDM cross-connects [4]–[12]. Such efforts include the joint switching of spatial superchannels [4]–[9] and a subsystem-modular wavelength cross-connect (WXC) architecture [10]–[12]. However, historically speaking, when a new signal multiplexing technology emerges, it needs a new networking layer and hence a new switching technology with the same switching granularity as the multiplexing granularity of the new layer to achieve cost-effective and scalable networking. In the same way that the introduction of WDM required an *optical bypass* based on ROADMs/WXCs when entering the WDM era in the early 2000s, SDM will need a *spatial bypass* based on spatial cross-connects (SXCs) to achieve a cost-effective SDM layer.

Here, let us consider the important question of when will the *spatial bypass* yield technological and economic validity. Based on the extrapolation of recent compound annual growth rates of high-end router blades, which is at approximately 40%, and other technologies used to generate and process data, Winzer *et al*. recently predicted that by around 2024 commercial 10-Tb/s optical interfaces will be required in 1-P b/s optical transport systems [3], [13]. Since a 10-Tb/s dual polarization quadrature phase shift keying (DP-QPSK) optical channel occupies almost the entire capacity of the C-band, it is abundantly clear that for such an ultra-high capacity optical channel, the wavelength switching layer is obsolete and the *spatial bypass* yields significant benefits in terms of cost-effectiveness and expanded optical reach due to simpler optical spatial switches.

Manuscript received February 4, 2020; revised April 23, 2020 and May 28, 2020; accepted June 2, 2020. Date of publication June 8, 2020; date of current version September 15, 2020. This work was supported in part by the JSPS KAKENHI under Grants 26220905 and JP18H01443, and in part by the National Institute of Information and Communication Technology (NICT) under Grants 19302 and 20401. *(Corresponding author: Masahiko Jinno.)*

The authors are with the Faculty of Engineering and Design, Kagawa University, Takamatsu 761-0396, Japan (e-mail: jinno@eng.kagawa-u.ac.jp; tkodama@eng.kagawa-u.ac.jp; s16t284@stu.kagawa-u.ac.jp).

Color versions of one or more of the figures in this article are available online at https://ieeexplore.ieee.org.

Digital Object Identifier 10.1109/JLT.2020.3000304

According to the aforementioned considerations, we recently proposed a novel optical network architecture, the spatial channel network (SCN), toward the forthcoming era of massive SDM [14]–[22]. In the SCN, the current optical layer is explicitly evolved into the hierarchical SDM layer and WDM layer, and a conventional optical node is decoupled into a SXC and a WXC to form a hiera rchical optical cross-connect (HOXC) [14], 1[6]. By doing so, future ultra-high capacity optical channels, which will have a bit rate of 10 Tb/s and beyond, will be able to bypass the overlying WXCs in the WDM layer (spatial bypass) using potentially inexpensive and low insertion loss SXCs. This yields significant reduction in the routing cost-per-bit in an optical transport network [16], [17] and considerable increase in the optical reach [15], [16]. We define a spatial channel (SCh) as an ultra-high capacity optical data stream that occupies the entire available spectrum of a core (C-band and/or L-band) in a conventional SMF or currently under development MCF. Hereafter, we refer to such a core as a spatial lane (SL). The introduction of MCFs may be the first technological step beyond the use of conventional SMF bundles for SDM links.

As SXC architectures with growability and reliability, our research group recently proposed novel SXC architectures [14], [16] based on a sub-matrix switch and a new type of optical spatial switch, which is referred to as a $1 \times k$ core selective switch (CSS). Recently, we demonstrated the feasibility of spatial channel networking including spatial bypassing, spectral grooming, spatial-lane change, and spatial-channel protection over a spatial channel network testbed that comprised two types of low-loss SXC prototypes connected with four-core fibers [18], [19].

Fig. 1(a) shows an HOXC architecture example comprising a CSS-based SXC and a conventional WXC. A CSS in an SCN provides functions equivalent to those provided by a conventional WSS in a current WDM network. Here, ingress and egress CSSs linked to MCF transmission lines are arranged in the *route and select* (R&S) configuration instead of the simpler *broadcast and select* (B&S) configuration. This is to avoid the inherent splitting loss of the optical splitter used in the B&S configuration and to achieve a low insertion loss SXC that actualizes an optical reach for a spectrally groomed optical channel (OCh) in an SCN that is almost the same as the optical reach in a current WDM network [15], [16]. In order to pack optical (wavelength) channels efficiently into an SCh, a conventional WXC is connected to add/drop ports of the SXC via spatial multiplexers (SMUXs) and spatial demultiplexers (SDEMUXs).

It should be noted that in the same way that a conventional WSS-based ROADM does not provide the wavelength conversion functionality, a CSS-based SXC does not provide the SL change (core interchange) functionality. Many studies have been performed to investigate the impact that wavelength contention has on the performance of optical-bypass-enabled networks and these studies concluded that there is only a small impact if good algorithms are used [22]. Similarly, we recently showed that the lack of lane change capability exerts little influence on the required number of SLs in the network (1% to 12% increase for incremental traffic demand depending on network topology when compared to the traditional Clos network based SXC) [17],

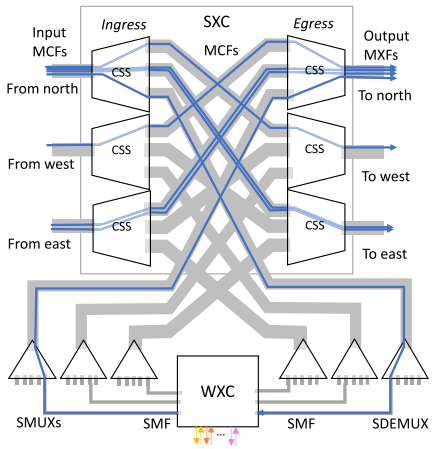

(a) HOXC architecture based on CSS

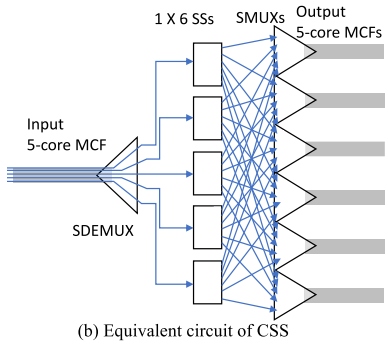

(b) Equivalent circuit of CSS

Fig. 1. SXC architecture based on $1 \times k$ CSS.

[23]. The few percent increase in the required number of SLs may be acceptable for a potentially lower node cost in CSS-based SXC architectures. There are a wide variety of add/drop part architectures and technologies to achieve more flexible connectivity in a CSS-based SXC at the expense of increased node complexity. Such architectures and techno-economic analysis are found in [23].

A $1 \times k$ CSS incorporates functionalities for spatially demultiplexing SChs from an input MCF and for switching and multiplexing any of them into any of k output MCFs. Connectivity is independent of the propagation direction of the SChs. Such functionality can be achieved by configuring an SDEMUX, $1 \times k$ spatial switches, and SMUXs as shown in Fig. 1(b). A feasibility demonstration for a CSS employing discrete bulk optics comprising MCF SMUX/SDEMUX devices and commercial 1×4 spatial switches was recently conducted [20]. In the demonstration, a preliminary switching experiment for a free-space-optics based CSS was also performed using an input MCF collimator and an output MCF collimator, which was affixed to a two-dimensionally movable stage to emulate multiple adjacently arranged output MCF collimators. More recently, a compact, free-space-optics based 5-core 1×6 CSS prototype with integrated input and output MCF collimators and an SMUX/SDEMUX array was reported in [21].

This paper is an expanded version of [21] in which detailed descriptions are added of the operational principle of a CSS

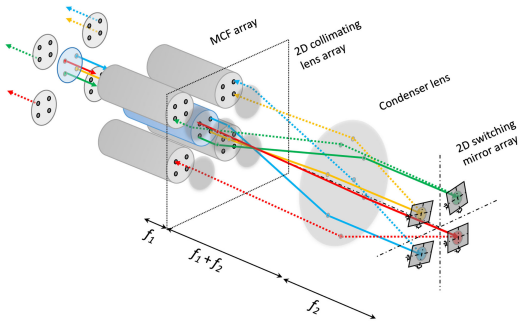

(a) Free-space-optics based architecture of 1 × 4 CSS

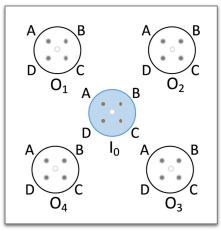

(b) Indexing of cores and MCFs

Fig. 2. Free-space-optics based architecture of 1×4 CSS.

with comparison to a conventional WSS, design parameters, system trade-offs in implementing a free-space-optics based CSS, and detailed experimental results of the 1×6 CSS prototype. The remaining part of this paper is structured as follows. In Section II, we describe the principle of the free-space based CSS. In Section III, we discuss the design for free-space based CSSs that support various numbers of cores and MCF ports. In Section IV, we show an example of an implemented 5-core 1×6 CSS prototype. In Section V, we present experimental results including the experimental configuration for a feasibility demonstration of spatial channel networking including using 100-Gb/s to 900-Gb/s spectral superchannels and experimental results. In Section VI, we summarize our conclusions.

II. Principle of Free-Space-Optics Based CSS

A free-space-optics based CSS was first proposed in our previous work [20]. To facilitate reader understanding of the free-space-optics based CSS, we describe in the first half of this section the basic principle of the CSS, which appeared in [20], and then provide detailed discussion of the features of the CSS compared to those of the conventional WSS. In Fig. 2(a), we illustrate a 1×4 CSS based on free-space optics that supports MCFs with four cores. The CSS comprises two-dimensionally arranged input and output MCFs with collimating micro-lenses whose focal length is f_1, a condenser lens whose focal length is f_2, and two-dimensionally arranged switching mirrors. Fig. 2(b) shows indexes for each MCF and each single mode core in an MCF, where cores are indexed using labels of A-D and MCFs are indexed using I_0 (input MCF) and O_1-O_4 (output MCFs). The collimating micro-lens and condenser lens are arranged in a telecentric configuration. The micro-lens for the input MCF collimates four beams (red, green, blue, and yellow) launched from each core of the input MCF and concentrates them to the focal point of the collimating lens at different angles according to the position of each core in the cladding. The condenser lens focuses each beam on a different switching mirror according to each angle. As a result of the telecentric configuration, the four spots on the switching mirrors appear as a point-symmetric enlarged image of the beam profiles at the cores of the input MCF with magnification factor M given by f_2/f_1. As illustrated using dotted traces, a beam from any core of the input MCF can be coupled to a core with the same core index of any output MCF by adjusting the tilt of each switching mirror in two angular dimensions. Fig. 2(a) illustrates a case where a beam from core A of the input MCF is coupled to core A of output MCF O_4, beams from cores B and C are respectively coupled to cores B and C of output MCF O_2, and a beam from core D is coupled to core D of output MCF O_1.

As described in [20], since the propagation directions of the lights are opposite between the input MCF and the output MCFs, the same core index at the input-end of an output MCF means that the switched light at the output end of the output MCF appears in the core in the horizontally-flipped position. Fortunately, if the R&S configuration is employed as shown in Fig. 1(a), this horizontal-flipping in the core position that occurs at an ingress CSS by routing the light can be restored to the original core position by selecting the light at an egress CSS. As a result, an SXC using the free-space-optics based CSSs provides the connection between cores with the same index if the R&S configuration is employed.

Higher level functionalities that a $1 \times k$ CSS provides are very similar to those that a $1 \times k$ WSS provides; however, there exist some important differences between them. First, a WSS needs a discrete diffraction grating for wavelength demultiplexing/multiplexing, which makes a WSS relatively bulky and lossy, while in a CSS, a collimator lens with negligibly small insertion loss doubles as a spatial demultiplexer/multiplexer. Second, because in the envisioned SXC applications a functionality that changes seamlessly the switching range, which is needed for flexible-grid-enabled WSSs and can only be achieved using a pixel-based liquid-crystal-on-silicon (LCoS) spatial light modulator (SLM), will most likely not be required. Alternatively, two-dimensionally arrayed micro-electro-mechanical-system (MEMS) mirrors that outperform an LCoS-SLM in terms of larger switching angles and polarization independency can be employed as a switching element. These two features are advantageous in decreasing the size and insertion loss of a CSS. Third, in a standard WSS design, switching mirrors are one-dimensionally arranged in the wavelength direction and input/output SMFs are arranged in the orthogonal direction, while in a CSS, both switching mirrors and input/output MCFs can be arranged two-dimensionally, which makes it relatively easy to support larger numbers of SLs and to increase the input/output MCF count. For example, if the maximum steering angle for an employed switching mirror supports N MCF ports in one direction in the Cartesian coordinate, we can support N^2 MCF ports in total by adjusting the tilt of the switching mirror in two angular dimensions.

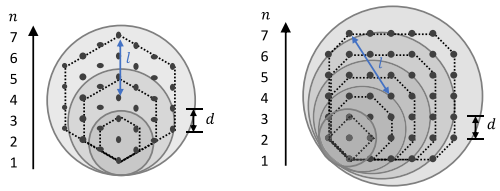

(a) Hexagonal closely-packed structure (b) Square lattice structure

Fig. 3. Core arrangement in hexagonal closely-packed MCFs and square lattice MCFs.

TABLE I
TOTAL CORE COUNT FOR N EQUALING 3 TO 7

n	Hexagonal close-packed		Square lattice	
	Core count	l/d	Core count	l/d
3	7	1	5	1
4	-	-	12	1.58
5	19	2	21	2.24
6	-	-	32	2.92
7	37	3	45	3.61

III. DESIGN OF FREE-SPACE OPTICS BASED CSS

A CSS was modeled as a telecentric imaging system with two-dimensionally (2D) arranged MCFs each coupled to a thin micro-lens (focal length f_1), a thin condenser lens (focal lengths f_2), and a switching mirror device array. So far, a wide variety of core arrangements have been reported in literature, including the hexagonal closely-packed structure and the square lattice structure [2], [24], [25]. Figs. 3(a) and 3(b) illustrate examples of the core arrangement in hexagonal closely-packed MCFs and square lattice MCFs, respectively. Here, we introduce index n that is a one-dimensional core count in an MCF. Table I summarizes the total core count for n equaling 3 to 7.

A. MCF Input/Output Array Design

Fig. 4(a) shows exemplary MCF geometry that has hexagonally closely-packed 7 single-mode cores. We assume a squarely arranged MCF and micro-lens arrays with micro-lens pitch D as shown in Fig. 4(b), whose per side MCF port count N is 4 and thus the total MCF port count N^2 is 16.

Fig. 4(c) shows a beam propagation model from the input MCF facet to the collimating micro-lens for the center core and outer cores. If we use a Gaussian beam as a model for light exiting from each core of the input MCF, where each beam has beam waist w_0 at the exit facet of each core and wavelength λ, the spot size on the micro-lens w_{col} is given by $\sqrt{w_0^2 + (\lambda f_1/\pi w_0)^2}$. The effective aperture of the micro-lens D_1 is determined so as to prevent significant beam clipping for beams emitted from the outermost cores. The required D_1 is given by $D_1 \geq 2(\alpha_1 w_{col} + l)$. Here, l is the length from the center of the MCF to an outermost core, which is given using n and core pitch d as $l = d(n-1)/2$ for hexagonal closely-packed structure MCFs and $l = d\sqrt{(n-1)^2 + (n-3)^2}/2$ for square lattice structure MCFs as shown in Figs. 3(a) and 3(b), respectively.

If we need the beam clipping for beams emitted from the outermost cores to be less than 1%, α_1 should be greater than 1.5. All beams launched from each core of an input MCF converge to the same spot at the focal point of the collimator lens at different angles and are spatially separated as shown in Fig. 4(d).

B. Steering Optics Design

Fig. 5(a) shows a side view schematic of the CSS. The three solid lines indicate beam propagations from the center and outer cores in the input MCF, which is located at the bottom left corner of the MCF array, to switching mirror devices. Dotted lines indicate possible beam propagations from the switching mirror devices to the output MCFs. Both an MEMS mirror array and an LCoS-SLM can be used as a switching mirror device array. Although additional polarization diversity optics are required for the latter case to compensate for the polarization dependency of the switching efficiency, it is omitted from Fig. 5(a) for better visibility.

If we assume that micro-lens pitch D is equal to the effective aperture of the micro-lens D_1 the effective aperture of the condenser lens D_2 is determined so as to prevent significant beam clipping for beams emitted from (entering into) the outermost cores of the MCFs located at the outermost corners. The required D_2 is given by $D_2 \geq 2\{\alpha_2 w_{con} + Ml + (N-1)D_1/\sqrt{2}\}$ where w_{con} is the spot size on the condenser lens given by $\sqrt{(\lambda f_1/\pi w_0)^2 + (M w_0)^2}$ and where α_2 should be greater than 1.5 to prevent the beam clipping of less than 1% by the condenser lens for the outermost beams.

The condenser lens focuses the beams on the switching mirror devices to generate a point-symmetric enlarged image of the beam profiles on the input MCF facet with magnification factor M given by f_2/f_1 This means that the spot size on the mirror device, w_{mir}, is given by Mw_0, as illustrated in Fig. 5(b) for an MEMS mirror array and Fig. 5(c) for an LCoS-SLM. Pitch R and effective radius r of the mirror devices should be Md and $\beta M w_0$, respectively, where β should be greater than 1.5 to ensure that the beam clipping by the switching mirror device for each beam is less than 1%.

The required maximum steering angle of the mirror device depends on N and has the relationship $f_2 \tan(\theta_{max}) \geq (N-1)\ D/2$. In other words, given core pitch d, mirror pitch R, and maximum steering angle θ_{max}, achievable per side MCF port count N_{max} and required minimum aperture $D_{1,min}$ with focal length f_1 of the collimating micro-lens are determined as a function of n and f_2 as

$$N_{max}(n, f_2) = \frac{2 f_2 \tan\theta_{max}}{D_{1,min}} + 1 \tag{1}$$

$$D_{(1,min)}(n, f_2) = 2\left\{\alpha_1 \sqrt{\left(w_0^2 + (\lambda d f_2)^2 / (\pi w_0 R)^2\right)} + l\right\}$$

$$\begin{cases} l = d(n-1)/2 & \text{(Hexagonal close - packed)} \\ l = d\sqrt{\left((n-1)^2 + (n-3)^2\right)}/2 & \text{(Square lattice)} \end{cases} \tag{2}$$

$$f_2 = (R/d)\ f_1 \tag{3}$$

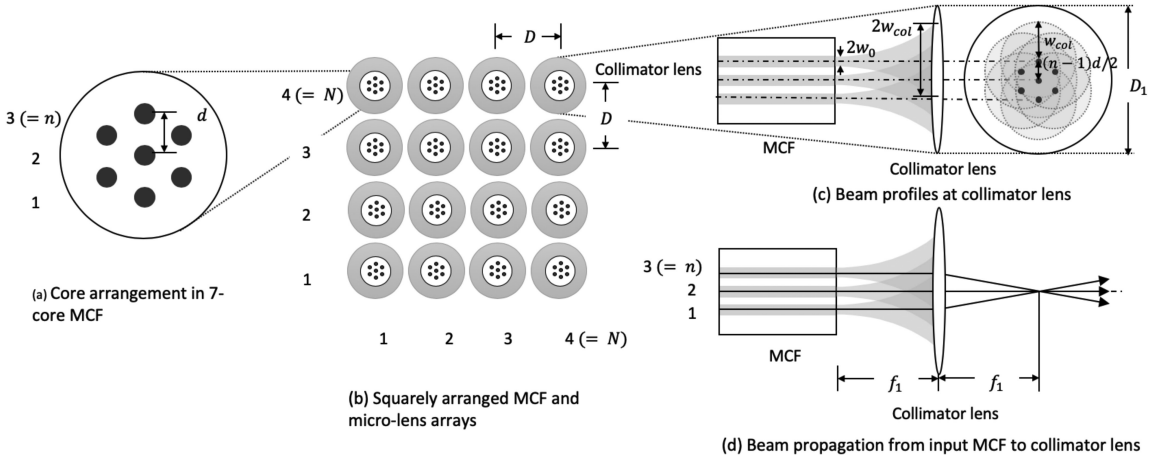

Fig. 4. MCF collimator array and beam propagation.

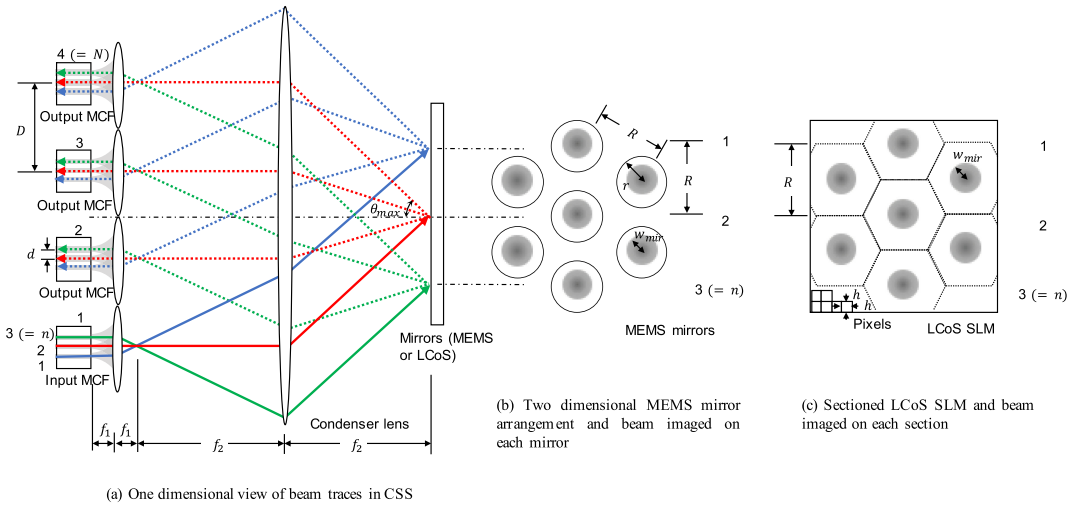

Fig. 5. Side view schematic of CSS, 2D MEMS mirrors, and sectioned LCoS-SLM.

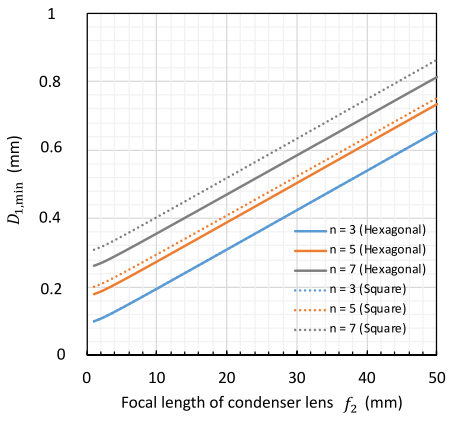

Fig. 6. Required minimum micro-lens aperture.

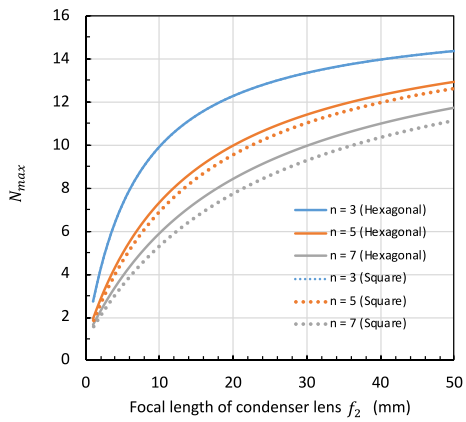

Fig. 7. Achievable per side MCF port count.

A large n and thus a large number of coresper fiber leads to a decrease in N_{max}. As f_2 increases, per side MCF port count N_{max} increases and approaches $M(\pi w_0/\alpha_1\lambda)\tan\theta_{max}+1$. Since f_2 is the chief parameter to determine the overall size of a CSS, if a sufficiently large θ_{max} to achieve the necessary port count, N_{max}, is available by using an MEMS mirror array with

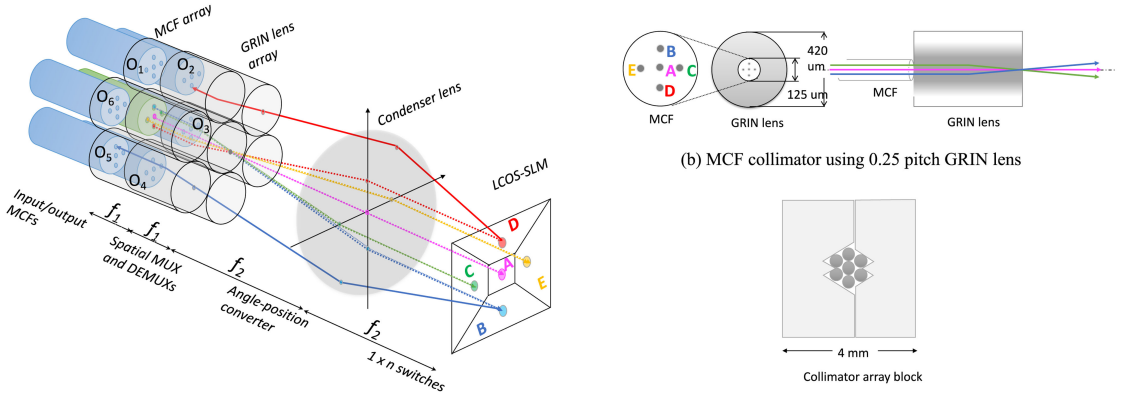

(a) Free-space-optics based 1×6 CSS prototype using LCoS-SLM

(b) MCF collimator using 0.25 pitch GRIN lens

(c) Seven MCF collimators arranged in hexagonal closely-packed structure

Fig. 8. Schematic diagram of CSS prototype supporting 5-core MCFs with standard 125-μm cladding.

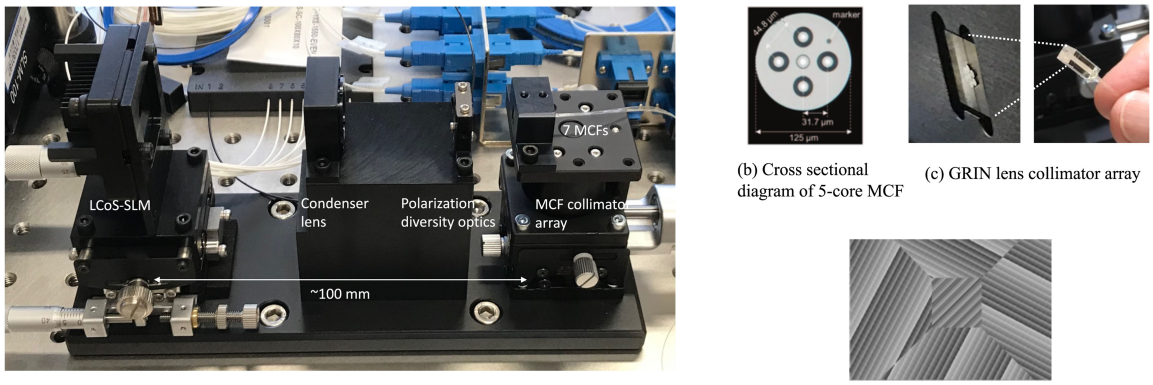

(a) Overall image of 5-core 1 x 6 CSS prototype

(b) Cross sectional diagram of 5-core MCF

(c) GRIN lens collimator array

(d) 2π saw-tooth hologram in sectioned LCoS-SLM

Fig. 9. Images of CSS prototype.

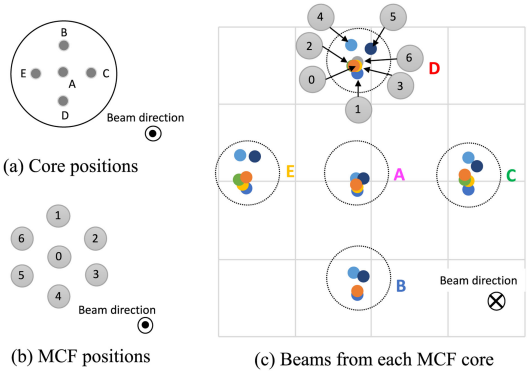

(a) Core positions

(b) MCF positions

(c) Beams from each MCF core

Fig. 10. Beams from each MCF core focused at LCoS position.

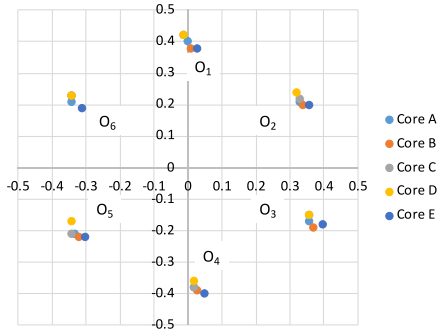

Fig. 11. Optimum steering polar and azimuthal angles (deg.).

a large mirror tilt angle, a shorter f_2 may be better. However, in practice, there exists a practical lower limit to f_2 because a shorter f_2 requires a shorter f_1 $(= f_2(d/R))$, but as can be understood from Eq. (2), required minimum aperture $D_{1,min}$ is not reduced at the same pace as f_2, and will never become less than $2\,(\alpha_1 w_0 + l)$. This makes the requirement for the collimator micro-lens for an excessively shorter f_2 unrealistic.

C. CSS Design Examples

Fig. 6 shows the required minimum aperture of a micro-lens, $D_{1,min}$, as a function of the focal length of the condenser lens, f_2 $(= (R/d)f_1)$, for $n = 3$, 5, and 7, which correspond to examining hexagonally closely-packed 7-core, 19-core, and 37-core MCFs and square lattice 5-core, 21-core, and 45-core MCFs, respectively. Here, we assume an MEMS mirror array

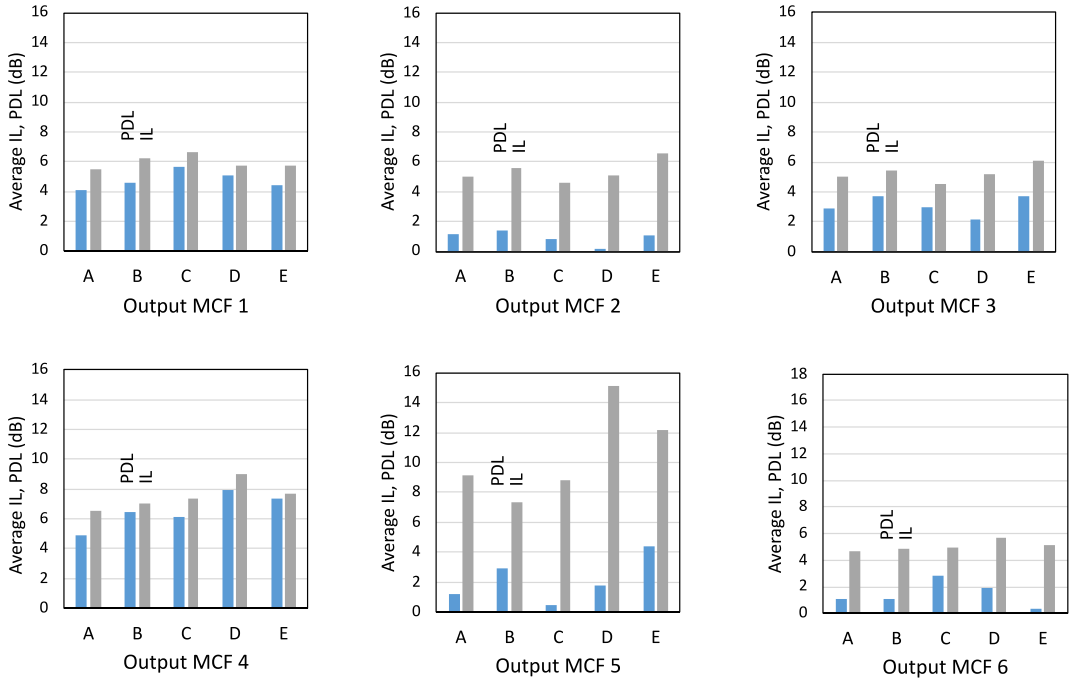

Fig. 12. IL η_{IL}, which is the ratio of the coupled power to the target core, P_t, and input power P_0, and the PDL at 1550 nm.

with $R = 1$ mm, $r = 0.3$ mm [26], and $\theta_{max} = \pm 5°$, and MCFs with $w_0 = 5.5$ μm, $d = 40$ μm, $\lambda = 1.55$ μm, and $\alpha_1 = 1.6$. Fig. 6 shows that the required minimum aperture of a micro-lens, $D_{1,min}$, increases with n and MCFs with square lattice cores require a slightly larger $D_{1,min}$ than MCFs with hexagonally closely-packed cores. Fig. 7 shows the maximum achievable per side MCF port count, N_{max}, as a function of f_2, when micro-lenses are closely arranged so that lens-pitch D equals $D_{1,min}$. Term N_{max} increases with f_2 and a larger n value (then larger core count) leads to a smaller N_{max} value due to a larger required minimum aperture, $D_{1,min}$.

Considering the case of micro-lens focal length f_1 of 810 μm ($f_2 = (R/d)f_1 = 20.3$ mm), Figs. 6 and 7 indicate that for hexagonally closely-packed 37-core MCFs ($n = 7$), the required minimum aperture, $D_{1,min}$, is 470 μm and the greatest integer less than or equal to N_{max} is 8. This means that the ideal case of a 37-core 1×63 CSS may be possible. If we use a micro-lens array with the same f_1 but a larger lens pitch, D, of 750 μm, which is a commercially available micro-lens design example, the achievable per side MCF port count, N, decreases to 5. This corresponds to a 37-core 1×24 CSS.

If we employ another MEMS design with twice the mirror pitch, $R = 2$ mm, twice the mirror radius, $r = 0.6$ mm, and the same commercially available micro-lens array design, we may achieve twice the per side MCF port count, N, that corresponds to a 37-core 1×99 CSS. This is at the expense of twice the f_2 of 40.6 mm and results in almost twice the device length.

On the other hand, a typical LCoS-SLM provides a much narrower steering angle, *e.g.*, $\theta_{max} = \pm 1.2°$, than an MEMS mirror. If we assume that an LCoS-SLM is divided into 19 sections and $R = 2$ mm, the achievable per side MCF port count, N, decreases to 3 for the same commercially available micro-lens array and the same condenser lens, which is still sufficient to achieve a 19-core 1×8 CSS.

IV. Implementing Free-Space-Optics Based CSS

In order to demonstrate the feasibility of a CSS, we constructed a free-space-optics based 1×6 CSS prototype using an LCoS-SLM [21] as illustrated in Fig. 8(a). As described in Section II, realistic SXC applications almost certainly do not need to change seamlessly the switching range, and two-dimensionally arrayed MEMS mirrors that outperform an LCoS-SLM in terms of larger switching angles and polarization independency may be preferable as a switching element. In this demonstration however, we employ an LCoS-SLM because of its beneficial programmable-configurability, which is advantageous especially in a laboratory, although it requires extra polarization diversity optics (not shown in Fig. 8(a) for better visibility).

The CSS prototype supports 5-core MCFs with a standard 125-μm cladding. The mode field diameter (MFD) and core spacing d of the MCF are 9 μm and 31.6 μm, respectively [24]. An MCF collimator was constructed by attaching a MCF to a 0.25-pitch graded-index (GRIN) lens as shown in Fig. 8(b), whose effective focal length f_1, effective lens diameter D_e, and outer diameter D_1 are 530 μm, 250 μm, and 420 μm, respectively. Rotational and translational alignment of a MCF and a GRIN lens is achieved by monitoring the collimated beam spot positions for the center core and outer cores. Seven MCF collimators are arranged in the hexagonal closely-packed structure as shown in Fig. 8(c) with the same rotational core arrangement to achieve an integrated input and output MCF collimator array. Here, each MCF and each core in the MCFs is indexed using labels of input MCF I_0 (center MCF), output

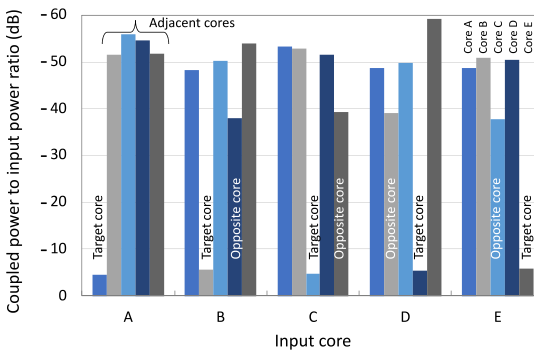

Fig. 13. Coupled power to input power ratio for output MCF O_2.

MCF O_1-O_6 (outer MCFs), core A (center core), and cores B-E, (outer cores) as shown in Fig. 8(a).

The GRIN lens collimates five beams from five cores of the input MCF and concentrates them at the end of the GRIN lens. Since the center core position coincides with the optical axis of the lens, the beam from the central core propagates straight along the optical axis of the lens while the beam from an outer core is launched at polar and azimuthal angles corresponding to the position of the core in the cross section of the MCF. This means that the collimating lens attached to the MCF acts as a spatial multiplexer and demultiplexer. A condenser lens with focal length f_2 of 50 mm is set to form a telecentric configuration with the collimator lenses.

Beams from each core of the input MCF focus on different positions at an LCoS-SLM according to their emitting angle at the end of the GRIN lens. The five spots on the LCoS-SLM represent a point-symmetric enlarged image of the MCF cores with magnification factor f_2/f_1. The LCoS-SLM is partitioned into five areas. The direction and period of the 2π saw-tooth hologram in each LCoS area is controlled so that each beam from the input MCF is directed independently to a core with the same index in its designated output MCF (*core selective switching*).

Fig. 9(a) shows anoverall image of the 5-core 1×6 CSS prototype employing an LCoS-SLM (Santec Corporation SLM-100). Figs. 9(b), 9(c), and 9(d) show the cross-sectional image of the 5-core MCF, an image of an integrated GRIN lens collimator array, and 2π saw-tooth hologram in the sectioned LCoS-SLM, respectively. Since an integrated GRIN lens array serves both as collimator lenses and SMUX/SDEMUXs, the CSS prototype is very compact in the order of double the focal length of the condenser lens (50 mm) and the size of the LCoS (10 mm $\times$ 15 mm). As described in the previous section, the achievable port count per fiber basically increases in proportion to the square of maximum steering angle θ_{max} of the switching element, and a larger port count CSS may be achieved by employing a two-dimensional MEMS array.

V. Performance Evaluation of CSS Prototype

A. Static Characteristics of CSS Prototype

If all the MCF collimators are constructed and arranged ideally, and a beam is emitted from a core of an output MCF instead of the input MCF, the beam should be focused on the same position on the surface of the LCoS-SLM where a beam launched from a core of the input MCF with the same index is focused. Fig. 10 shows beams from each MCF core focused on the LCoS position, which is observed by using a spatial beam profiler placed at the LCoS position while launching a continuous lightwave at 1550 nm into each core of each MCF. Each beam spot position corresponds to the core position in the cladding from which the beam originates. Discrepancies in the beam spot position for each core, especially seen for MCFs O_4 and O_5, indicate the imperfection of the GRIN-MCF alignment. This results in greater insertion loss (IL) and/or greater polarization dependent loss (PDL) due to the polarization-dependent beam clipping via the polarization diversity optics. We search the optimum steering polar and azimuthal angles for each core to connect to each output MCF by monitoring the coupled optical power while horizontally and vertically sweeping the pitch of the 2π saw-tooth hologram in the sectioned LCoS-SLM. Fig. 11 shows the optimum steering polar and azimuthal angles in degrees for each core to connect to output MCFs $O_1 \sim O_6$. Each position in the polar-angle and azimuthal-angle plane corresponds to the position of the output MCF in the MCF array.

Fig. 12 shows the IL and the PDL at 1550 nm [21]. The IL includes the excess loss of the fan-in/fan-out devices [27] used for the IL measurement (0.9 dB $\sim$ 1.4 dB in total) and the LCoS diffraction loss ($\sim$1 dB at the steering angle of $\sim$0.4°) when cores A$\sim$E of the input MCF are connected to output MCFs $O_1 \sim O_6$. Output MCFs O_1, O_4, and O_5 exhibit relatively high IL and/or PDL probably due to imperfect alignment as inferred from the results shown in Fig. 10. The minimum IL of 4.0 dB and PDL of 0.7 dB are achieved for core C of output MCF O_2. No wavelength-dependent loss is observed over the C-band. These observations indicate that the free-space-optics based CSS architecture will potentially provide low net IL at the level of approximately 2 dB for all output MCFs if the non-uniformity of the IL in the MCF collimators is improved as the manufacturing technology matures and a two-dimensional MEMS mirror array is employed instead of an LCoS-SLM.

Fig. 13 shows the coupled power to input power ratio for target core η_t and adjacent cores η_{adj} in the same output MCF O_2 expressed in decibels. Inter-core crosstalk (XT) XT is defined by the ratio of η_{adj} and η_t. Although most cores indicate low inter-core XT less than -43 dB, this is much higher than that expected from the simple formula of $XT \equiv \eta_{adj}/\eta_t = \eta_{adj} = \exp\{-(\mathrm{d}/w_0)^2\}$ for $d =$ 31.7 μm and $w_0 = 4.5$ μm (half the MFD). We attribute this discrepancy to unknown multiple stray lights. Relatively high inter-core XT from an outer core to a diagonal outer core at the level of approximately -33 dB is observed, which is considered to be caused by the unwanted reflection generated at the facet of the GRIN lens. This may be improved by applying antireflection coating to the GRIN lens facet.

Deviation from the ideal steering angle, $\Delta\theta$, causes incident angle deviation at the target core, and results in the decrease in the coupled power as indicated by $\eta_t(\Delta\theta) = \exp\{-((\pi w_0\, M\Delta\theta)/\lambda)^2\}$. The steering angle deviation also causes the incident angle deviation at the adjacent core in the same output MCF and results in the decrease in

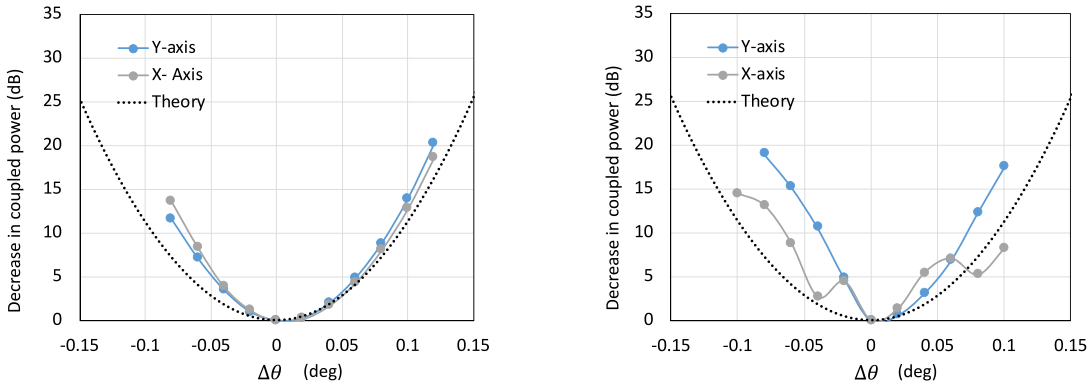

(a) Target core (center core in O_2) (b) Adjacent core (upper core in O_2)

Fig. 14. Decrease in coupled power for target and adjacent cores as a function of deviation from the ideal steering angle.

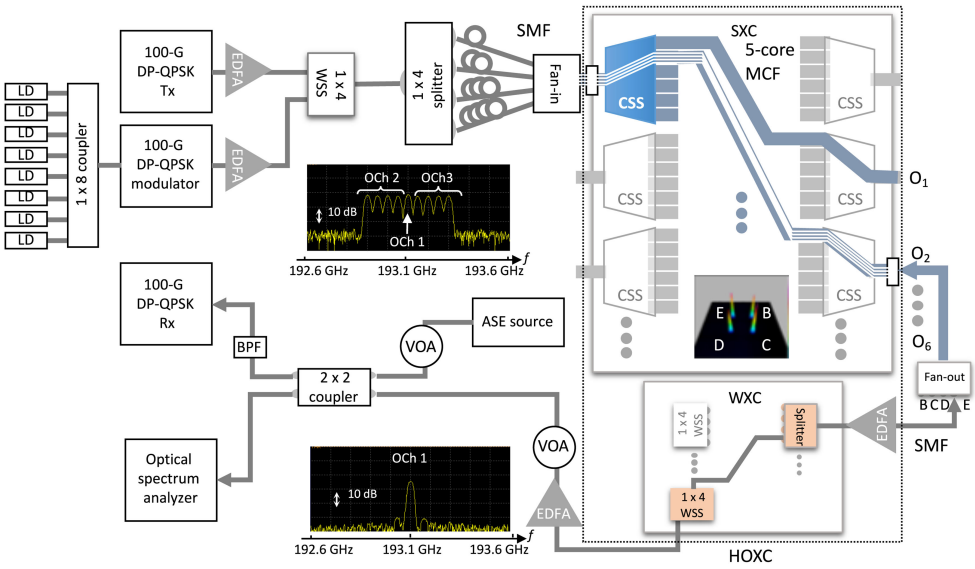

Fig. 15. Experimental configuration to measure BER performance of CSS prototype.

the coupled power to an adjacent core as $\eta_{adj}(d, \Delta\theta) = \exp\{-(\mathrm{d}/w_0)^2 - ((\pi w_0\, M\Delta\theta)/\lambda)^2\}$. This means the ratio of coupled powers to the adjacent and target cores (inter-core XT) does not increase even when there is deviation from the ideal steering angle and remains as $XT = \eta_{adj}/\eta_t = \exp\{-(\mathrm{d}/w_0)^2\}$. We experimentally confirmed this by intentionally shifting the steering angle for switching in both the x and y directions and observing the decrease in the coupled power to the target core and the adjacent cores as shown in Figs. 14(a) and 14(b), respectively.

B. Data Transporting Characteristics of CSS Prototype

In order to confirm that there are no unknown deteriorating factors in the CSS prototype, we tested the CSS prototype implemented in an HOXC [21]. We employ the simplest but most restrictive connectivity configuration, i.e., the *directional* and *fixed-core-access* configuration, in the SXC design [23] where each WXC port has a fixed link to a dedicated core in a dedicated ingress/egress MCF port. We measured the pre-forward error correction (FEC) bit error rate (BER) under the conditions below.

A) A single 100-Gb/s DP-QPSK signal is switched by the CSS to output MCFs $O_1 \sim O_6$.

B) Four 100-Gb/s DP-QPSK signals with the same carrier frequency that are spatially multiplexed and each propagating in a different outer core of a 5-core MCF are switched by the CSS to the same output MCFs, $O_1 \sim O_6$.

C) Four spectrally multiplexed single 100-Gb/s DP-QPSK signals and two 400-Gb/s DP-QPSK signals that are spatially multiplexed and each propagating in a different outer core of a 5-core MCF are switched by the CSS to the same output MCFs, $O_1 \sim O_6$, and groomed by a WXC.

Fig. 15 shows the experimental configuration for the pre-FEC BER measurement in the HOXC based on the CSS prototype. Figs. 16(a), 16(b), and 16(c) show the optical signal-to-noise ratio (OSNR) penalty at the $BER = 1 \times 10^{-3}$ for 100-Gb/s

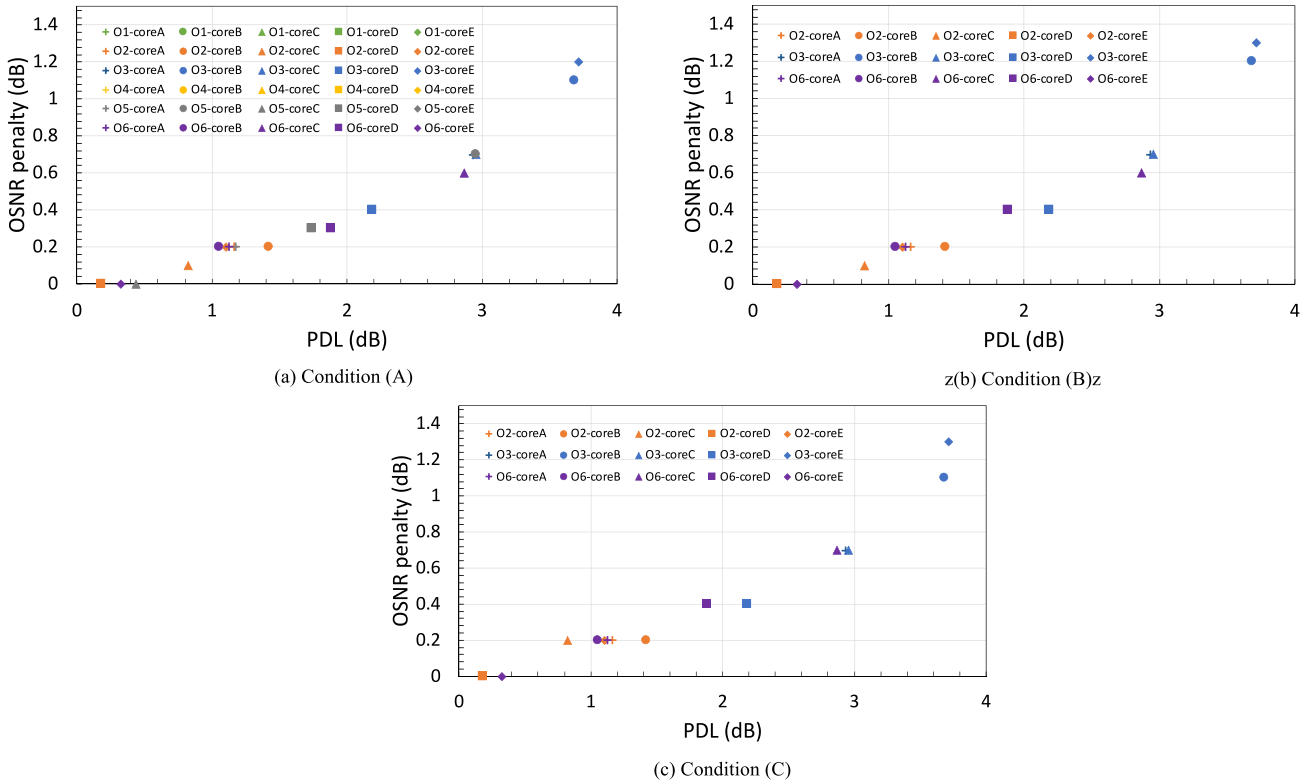

Fig. 16. OSNR penalty observed under conditions (A)∼(C).

DP-QPSK signals under conditions (A), (B), and (C), respectively, as a function of the PDL that they experienced. If we compare Figs. 16(b) and 16(c) to Fig. 16(a), we can see that the OSNR penalty only increases as the PDL increases. Neither the inter-core XT (Fig. 16(b)) nor spectral grooming (Fig. 16(c)) causes an increase in the OSNR penalty. This indicates that we can expect a negligible OSNR penalty for all CSS connections if GRIN-MCF alignment is improved.

VI. Conclusion

We described the principle, design, and prototyping of a free-space-optics-based CSS. In an SCN, a $1 \times k$ CSS provides functions equivalent to those provided by a conventional WSS in a current WDM network and incorporates functionalities for spatially demultiplexing SChs from an input MCF and for switching and multiplexing any of them into any of k output MCFs. We discussed the design for free-space-optics based CSSs that is applicable to CSSs supporting various numbers of cores per MCF and various numbers of MCF ports. We prototyped a 5-core 1×6 CSS that comprises an integrated MCF collimator, SMUX/SDEMUX array, and an LCoS-SLM. Although some output MCF ports exhibited relatively high IL, the CSS prototype successfully showed that a CSS potentially provides low net IL at the level of approximately 2 dB.

Since in our CSS design, a collimator lens with negligibly low IL doubles as an SMUX/SDEMUX and two-dimensionally arrayed MEMS mirrors with larger switching angles can be employed, the CSS potentially has advantages in terms of compactness, low-IL, and cost effectiveness. Although in this paper, a CSS prototype with relatively small numbers of cores and a MCF port count was described, since both switching mirrors and input/output MCFs can be arranged two-dimensionally meaning that the total numbers of them increase quadratically, we expect that it is relatively easy to support larger numbers of SLs and to increase the input/output MCF count if we employ more sophisticated input/output MCF array and micro-lens array assembly technologies.

Performance evaluation of the CSS prototype in an HOXC configuration including spatial bypassing and spectral grooming of a 900-Gb/s SCh successfully showed that the CSS enables a low-loss, distortion-free, and small foot-print SXC that will be needed in future SCNs in the forthcoming SDM era. Clearly, from the analogy of WSS-based WXC architectures, there must be a wide variety of CSS-based SXC architectures in terms of the connection flexibility in the add/drop part and novel optical spatial switches may be required to achieve such flexible SXCs [23]. Our future work will be to demonstrate the feasibility of flexible SXC architectures.

Acknowledgment

The authors would like to thank Furukawa Electric Co., Ltd. for their technical support related to the MCFs and fan-in/fan-out devices.

REFERENCES

[1] P. J. Winzer, "Scaling optical fiber networks: Challenges and solutions," *Opt. Photon. News*, vol. 26, no. 3, pp. 28–35, 2015.

[2] K. Saitoh, "Multicore fiber technology," *J. Lightw. Technol.*, vol. 34, no. 1, pp. 55–66, 2016.

[3] P. J. Winzer and D. T Neilson, "From scaling disparities to integrated parallelism: A decathlon for a decade," *J. Lightw. Technol.*, vol. 35, no. 5, pp. 1099–1115, Mar. 2017.

[4] D. M. Marom, N. K. Fontaine, Y. Ikuma, R. Proietti, L. Zong, J. M. Rivas-Moscoso, and I. Tomkos, "Survey of photonic switching architectures and technologies in support of spatially and spectrally flexible optical networking [invited]," *J. Opt. Commun. Netw.*, vol. 9, no. 1, pp. 1–26, 2017.

[5] M. D. Feuer, L. E. Nelson, K. Abedin, X. Zhou, T.F. Taunay, J. F. Fini, B. Zhu, R. Isaac, R. Harel, G. Cohen, and D. M. Marom, "ROADM system for space division multiplexing with spatial superchannels," OFC 2013, Paper PDP5B.8.

[6] L. E. Nelson, X. Zhou, T. F. Taunay, J. M. Fini, B. Zhu, R. Isaac, R. Harel, G. Cohen, and D. M. Marom, "Spatial superchannel routing in a two-span ROADM system for space division multiplexing," *J. Lightw. Technol.*, vol. 32, no. 4, pp. 783–789, Feb. 2014.

[7] D. M. Marom and M. Blau, "Switching solutions for WDM- SDM optical networks," *IEEE Commun. Mag.*, vol. 53, no. 2, pp. 60–68, Feb. 2015.

[8] N. K. Fontaine, T. Haramaty, R. Ryf, H. Chen, L. Miron, L. Pascar, M. Blau, B. Frenkel, L. Wang, Y. Messaddeq, S. LaRochelle, R. J. Essiambre, Y. Jung, Q. Kang, J. K. Sahu, S. U. Alam, D. J. Richardson, and D. M. Marom, "Heterogeneous space-division multiplexing and joint wavelength switching demonstration," OFC 2015, Paper Th5C.5.

[9] M. Jinno and Y. Mori, "Unified architecture of an integrated SDM-WSS employing a PLC-based spatial beam transformer array for various types of SDM fibers," *J. Opt. Commun. Netw.*, vol. 9, no. 2, pp. A198–A206, 2017.

[10] Y. Iwai, H. Hasegawa, and K. Sato, "A large-scale photonic node architecture that utilizes interconnected OXC subsystems," *Opt. Express*, vol. 21, no. 1, pp. 478–487, 2013.

[11] M. Niwa and K. Sato, "Tipping point for the future scalable OXC: What size M × M WSS is needed?" *J. Opt. Commun. Netw.*, vol. 9, pp. A18–A25, 2017.

[12] R. Hashimoto, H. Hasegawa, K. Sato, K. Yamaguchi, K. Seno, and K. Suzuki, "First demonstration of subsystem-modular optical cross-connect using single-module 6 × 6 wavelength-selective switch," *J. Lightw. Technol.*, vol. 36, no. 7, pp. 1435–1442, Apr. 2018.

[13] P. J. Winzer, D. T Neilson, and A. R Chraplyvy, "Fiber-optic transmission and networking: The previous 20 and the next 20 years," *Opt. Express*, vol. 26, no. 18, pp. 24190–24239, 2018.

[14] M. Jinno, "Spatial channel network (SCN) architecture employing growable and reliable spatial channel cross-connects toward massive SDM era," PSC 2018, Paper Fr3C.5.

[15] M. Jinno, "Added value of introducing spatial bypass into WDM/SDM networks: Gaussian-noise model analysis for spatially-bypassed and spectrally-groomed optical channels," ECOC 2018, Paper We3D.6.

[16] M. Jinno, "Spatial channel network (SCN): Opportunities and challenges of introducing spatial bypass toward massive SDM era [Invited]," *J. Opt. Commun. Netw.*, vol. 11, no. 3, 2019.

[17] M. Jinno and Y. Asano, "Required link and node resource comparison in spatial channel networks (SCNs) employing modular spatial channel cross-connects (SXCs)," OFC 2019, Paper M1A.1.

[18] M. Jinno, K. Yamashita, Y. Asano, R. Nakai, and D. Suzuki, "Demonstration of spatial channel networking using two types of hierarchical optical cross-connects," ECOC 2019, Paper Th1A.6.

[19] M. Jinno, T. Kodama, and T. Ishikawa, "Feasibility demonstration of spatial channel networking using SDM/WDM hierarchical approach for peta-b/s optical transport," *J. Lightw. Technol.*, vol. 38, no. 9, pp. 2577–2586, May 2020.

[20] M. Jinno, K. Yamashita, and Y. Asano, "Architecture and feasibility demonstration of core selective switch (CSS) for spatial channel network (SCN)," OECC/PSC 2019, Paper WA2.

[21] M. Jinno, T. Kodama, and T. Ishikawa, "Five-core 1 × 6 core selective switch and its application to spatial channel networking," OFC 2020, 2020, Paper M3F.3.

[22] J. M. Simmons, *Optical Network Design And Planning*, 2nd Ed., Berlin, Germany: Springer, 2013.

[23] M. Jinno, "Spatial channel cross-connect architectures for spatial channel networks," *IEEE J. Sel. Topics Quantum Electron.*, vol. 26, no.4, Jul./Aug. 2020, Art. no. 3600116.

[24] K. Aikawa, K. Takenaga, S. Matsuo, K. Saitoh, T. Morioka, and Y. Miyamoto, "High core count single-mode multicore fiber for dense space division multiplexing," in *Proc. IEEE Photon. Soc. Summ. Topic. Meetng. Ser.*, 2016, Paper WE2.2.

[25] T. Gonda, K. Kawasaki, S. Arai, R. Sugizaki, S. Beppu, D. Soma, H. Takahashi, and T. Tsuritani, "Design of multicore fiber having upgradability from standard single-mode fibers and its application," *J. Lightw. Technol.*, vol. 37, no. 2, pp. 396–403, Jan. 2019.

[26] D. T. Neilson, Paul Kolodner, C. A. Bolle, Roland Ryf, J. Kim, A. R. Papazian, C. J. Nuzman, A. Gasparyan, N. R. Basavanhally, V. A. Aksyuk, and J. V. Gates, "256 × 256 port optical cross-connect subsystem," *J. Lightw. Technol.*, vol. 22, no. 6, pp. 1499–1509, Jul. 2004.

[27] K. Kawasaki, T. Saito, and R. Sugizaki, "Four-fiber fan-out for MCF with square lattice structure," OFC 2017, Paper W3H.4.

Masahiko Jinno (Fellow, IEEE) received the B.E. and M.E. degrees in electronics engineering from Kanazawa University, Ishikawa, Japan in 1984 and 1986, respectively, and the Ph.D. degree in engineering from Osaka University, Osaka, Japan in 1995 for his work on ultra-fast optical signal processing based on nonlinear effects in optical fibers.

He currently serves as a Professor of the Faculty of Engineering and Design at Kagawa University, Takamatsu, Japan. His current research interests include architecture, design, management, and control of optical networks, optical transmission systems, optical cross-connects, optical switches, rate- and format-flexible optical transponders. Prior to joining Kagawa University in October 2012, he was a Senior Research Engineer and Supervisor at Nippon Telegraph and Telephone (NTT) Network Innovation Laboratories, NTT Corporation conducting pioneering research on spectrum- and energy-efficient elastic optical networks (EONs). From 1993 to 1994, he was a Guest Scientist at the National Institute of Standards and Technology (NIST), Boulder, Colorado, USA. He authored or co-authored over 180 peer-reviewed journal and conference papers in the fields of ultra-fast optical signal processing for high-capacity optical time division multiplexed transmission systems, optical sampling and optical time-domain reflectometry, ultra-wideband DWDM transmission systems in the L-band and S-band, ROADM systems, GMPLS and application-aware optical networking, EONs, and SDM networks.

Prof. Jinno is a Fellow of the Institute of Electronics, Information and Communication Engineers (IEICE) and a Member of the Optical Society of America (OSA). He received the Young Engineer's Award in 1993, the Best Tutorial Paper Award in 2011, the Best Paper Award in 2012, the Achievement Award in 2017, and the Milestone Certificate in 2017 from the IEICE, the best paper awards from the 1997, 1998, 2007, and 2019 Optoelectronics and Communications Conferences (OECC), the Best Paper Award from the ITU-T Kaleidoscope Academic Conference in 2010, and the Outstanding Paper Award in 2013 from the IEEE Communications Society Asia-Pacific Board.

Takahiro Kodama (Member, IEEE) received the B.E. degree from Ritsumeikan University, Shiga, Japan in 2008 and M.E. and Dr. Eng. degrees from Osaka University, Osaka, Japan in 2010 and 2012, respectively. In 2012, he was selected as a Research Fellow of the Japan Society for the Promotion of Science (JSPS). In 2014, he joined Mitsubishi Electric Corporation, Kanagawa, Japan. In 2016, he was a Research Assistant Professor with the Graduate Faculty of Interdisciplinary Research, University of Yamanashi, Yamanashi, Japan and was selected as an Excellent Young Researcher of the Ministry of Education, Culture, Sports, Science and Technology (MEXT) of Japan. Since 2019, he has been a Lecturer in the Faculty of Engineering and Design, Kagawa University. His research interests are in the area of optical access, metro and core network, optical packet switching network, digital signal processing, and optical signal processing. He has published over 50 papers in refereed journals and international conference papers.

Dr. Kodama is a member of the Institute of Electronics, Information and Communication Engineers (IEICE). He was the recipient of the 2011 IEEE Kansai Section Student Paper Award.

Tsubasa Ishikawa was born in Tokushima, Japan in 1998. He is currently a graduate student at Kagawa University.